

# Interaction of OAM light with Rydberg excitons: Modifying dipole selection rules

Annika Melissa Konzelmann,<sup>1</sup> Sjard Ole Krüger,<sup>2</sup> and Harald Giessen<sup>1\*</sup>

<sup>1</sup>4<sup>th</sup> Physics Institute and Research Center SCoPE, University of Stuttgart, Pfaffenwaldring 57, D-70569 Stuttgart, Germany

<sup>2</sup>Institut für Physik, Universität Rostock, Albert-Einstein-Straße 23, D-18059 Rostock, Germany

\*[h.giessen@pi4.uni-stuttgart.de](mailto:h.giessen@pi4.uni-stuttgart.de) <https://www.pi4.uni-stuttgart.de>

**Abstract:** Orbital angular momentum (OAM) light possesses in addition to its usual helicity ( $s = \pm\hbar$ , depending on its circular polarization) an orbital angular momentum  $l$ . This means that in principle one can transfer more than a single quantum of  $\hbar$  during an optical transition from light to a quantum system. However, quantum objects are usually so small (typically in the nm range) that they only locally probe the dipolar character of the local electric field. In order to sense the complete macroscopic electric field, we utilize Rydberg excitons in the semiconductor cuprite ( $\text{Cu}_2\text{O}$ ), which are single quantum objects of up to  $\mu\text{m}$  size. Their interaction with focused OAM light, allows for matching the focal spot size and the wavefunction diameter. Here, the common dipole selection rules ( $\Delta j = \pm 1$ ) should be broken, and transitions of higher  $\Delta j$  with higher order OAM states should become more probable. Based on group theory, we analyze in detail the optical selection rules governing this process.

## I. INTRODUCTION

Cuprous oxide ( $\text{Cu}_2\text{O}$ ) is a semiconductor which crystallizes in a cubic lattice ( $a = 4.26 \text{ \AA}$ ) and has a direct band gap of 2.17 eV (FIG. 1 (a)).<sup>1</sup> An exciton is an excited state of the crystal, in which an electron and a hole form a quasiparticle bound by Coulomb interaction. In covalent crystals, excitons are delocalized, the electron-hole pair is loosely bound, and the orbits are large ( $\sim 1\mu\text{m}$ ). The so-called Wannier excitons appear in the low energy spectrum of the crystal as sharp absorption peaks below the bandgap.<sup>2</sup> Cuprous oxide has in total ten valence and four conduction bands. The highest valence band is formed by copper 3d orbitals; the lowest conduction band is formed by copper 4s orbitals. Both bands have the same parity, thus the dipole moment between them vanishes. Therefore, electric dipole transitions between these bands for excitons with s-type envelope are forbidden and the radiative lifetimes of the Rydberg P-excitons are relatively long ( $\tau \approx \text{ns}$ ) due to the low energy relaxation rate, despite the fact that the large wave function extension may be confronted with multiple scattering possibilities in crystals. The energies of the optically excited P-excitons can be determined directly by one-photon absorption studies, in which the photon energy of a single-frequency laser with a narrow spectral linewidth of a few neV is continuously tuned. The exciton energy series can be calculated according to:  $E_n = E_g - Ry^*/(n - \delta_{n,l})^2$ , with the band gap energy  $E_g$ , the exciton binding energy  $E_B = Ry^*/(n - \delta_{n,l})^2$ , the quantum defect  $\delta_{n,l}$  induced by the non-parabolic hole dispersions,<sup>3</sup> and the modified Rydberg constant  $Ry^* = Ry \cdot m^*/(\epsilon^2 m)$ . The crystal environment is taken into account through the permittivity  $\epsilon$ , which is isotropic for cubic ( $O_h$ ) symmetry, and the effective electron and hole masses  $m_e$  and  $m_h$  are incorporated via  $m^* = m_e \cdot m_h / (m_e + m_h)$ . Exciton states with large principal quantum number  $n$  are termed Rydberg excitons and have macroscopic dimensions in  $\text{Cu}_2\text{O}$ . These states are well suited for the investigation of interaction effects. Huge polarizabilities are expected, leading to enormously strong dipolar interactions.<sup>4</sup> Furthermore, in contrast to Rydberg atoms, highly excited excitons with  $\mu\text{m}$ -size extensions are of interest because they can be placed and moved in a crystal with high precision using macroscopic energy potential landscapes.<sup>5</sup>

When we regard crystals as macroscopic continua, the rotational symmetry is broken down to discrete groups.<sup>6</sup> However, in cuprous oxide the symmetry is still quite high (point group  $O_h$ ). The symmetry transformations of a Hamiltonian always form a group, which is directly related to the physical symmetry of the system to which the Hamiltonian applies. Such symmetry considerations can be used to extract information residing in the respective transition matrix elements regarding the selection rules associated with OAM transfer. Optical transitions occur from the crystal ground state to the excitonic states and are driven by the light field operator. Any interaction between radiation and matter is inevitably accompanied by an exchange of momentum. Light beams with an azimuthal phase dependence of  $e^{-il\phi}$  carry an angular momentum independent of the polarization state.<sup>7-11</sup> For any given  $l$  the beam has  $l$  intertwined helical phase fronts, for which the Poynting vector has an azimuthal component, meaning it is no longer parallel to the beam axis. That component produces an orbital angular momentum parallel to the beam axis, which is associated with regions of high intensity, together with a phase singularity on the beam axis with zero optical intensity and no linear or angular momentum, that persists no matter how tightly the beam is focused. The most common form of helically phased beams are the Laguerre-Gaussian laser modes. Such donut modes form a complete basis set for paraxial light beams and have circular symmetry.

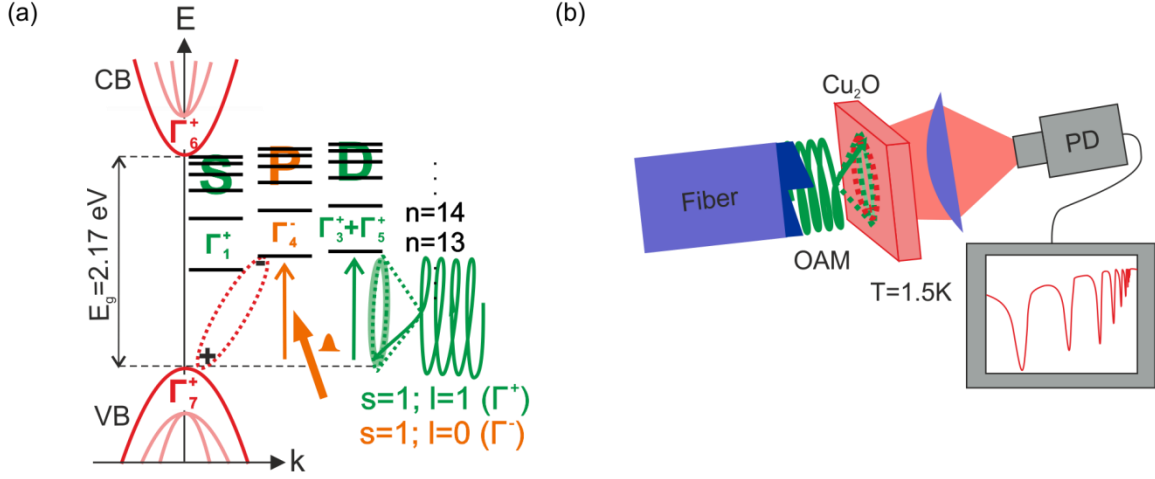


FIG. 1. (a) Formation of different exciton series between the highest valence (VB) and the lowest conduction (CB) bands in  $\text{Cu}_2\text{O}$  depending on the light properties ( $s = 1; l = 0, 1$ ). Using OAM light, Rydberg excitons with different envelope functions ( $S, P, D, \dots$ ) can be excited by allowed transitions. (b) Experimental scheme: A spiral phaseplate imprinted on a fiber facet creates OAM light, which excites Rydberg excitons in cuprite at cryogenic temperatures. The signal is detected using a photodiode. The Rydberg exciton series is visible in the absorption spectrum as broadened, asymmetric, Fano-shaped absorption lines.

## II. METHODS

Our aim is to predict whether an optical transition between the cuprite crystal ground state and exciton states with different amount of angular momentum  $l^{exc}$  is allowed or forbidden when exciting with OAM light. For allowed transitions the overlap of crystal ground and excited state contains the symmetry of the exciting light (optical transition driving operator  $\mathbf{A} \cdot \mathbf{p}$ ). The symmetries of the excitonic states are derived from the cuprous oxide band symmetries. In addition, as the excitation takes place inside the crystal, we use the tables of Ref. [12] to determine the OAM light symmetries within the symmetry group of the  $\text{Cu}_2\text{O}$  crystal.

Cuprous oxide belongs to symmetry group  $O_h$ , which contains all 24 proper and 24 improper rotations which transform a cube into itself. Knowing how the symmetry group behaves under parity, it suffices to take only the symmetry classes with the proper rotations into account. The symmetry of an exciton is described by the product of the symmetries of the conduction band (electron), the valence band (hole), and the envelope function, determining the angular momentum quantum state. The former two symmetries are known from literature<sup>13</sup> and the latter one can be derived from the atomic orbitals of the hydrogen wave function due to the high symmetry of cuprite.<sup>14–16</sup> Orbital angular momentum light is described by a Laguerre-Gauss mode, which can be decomposed, in the longitudinal dipole approximation, into a plane wave part  $\mathbf{A}_0$  times a phase factor  $e^{il\phi}$ . While the symmetry of the plane wave part is trivial, in order to extract the symmetry of the phase factor, we decompose the latter one into basis functions, analyze how these basis functions change when undergoing  $O_h$  symmetry operations and calculate the trace of the transformation matrix (characters). For the complete set of characters (one character per symmetry operation) the corresponding light field symmetry can be assigned according to the character tables of group  $O_h$ .<sup>12</sup>

## III. RESULTS AND DISCUSSION

### A. OAM light symmetry assignment via calculation of transformation matrix diagonal elements

In the following we are going to assign a symmetry to the optical transition driving operator involving OAM light modes with different amount of orbital angular momentum  $l$ . OAM light is described by a Laguerre-Gauss mode which is a Gaussian beam times an additional phase factor  $e^{il\phi}$ . The complete light field operator  $\mathbf{A}$  has the form:

$$\mathbf{A}_{lp}(r, \phi, z) = \mathbf{A}_0 e^{ikz} \frac{w_0}{w} \exp\left(\frac{-r^2}{w^2} + \frac{ikr^2}{2R} - i(2p + |l| + 1)\phi(z)\right) \cdot \left(\frac{\sqrt{2}r}{w}\right)^{|l|} L_p^{|l|}\left(\frac{2r^2}{w^2}\right) e^{il\phi}, \quad (1)$$

with  $\mathbf{A}_0$ : light field amplitude,  $k$ : wave vector,  $w(z)$ : beam waist,  $w_0 = w(z = 0)$ ,  $\phi(z)$ : Gouy phase,  $R(z)$ : radius of curvature,  $L_p^{|l|}$ : generalized Laguerre polynomial. In dipole approximation the Gaussian beam part simplifies to  $\mathbf{A}_0 e^{ikz} \approx \mathbf{A}_0 (1 + ikz) \approx \mathbf{A}_0$ . From the OAM part, the only relevant factor for symmetry considerations is  $e^{il\phi}$ . Then, the optical transition driving operator becomes  $\mathbf{A} \cdot \mathbf{p} = \mathbf{A}_0 \cdot e^{il\phi} \cdot \mathbf{p}$ . The symmetries of  $\mathbf{A}_0$  and  $\mathbf{p}$  with respect to group  $O_h$  are  $\Gamma_1^+$  and  $\Gamma_4^-$ , respectively. The function  $e^{il\phi}$  is cylindrically symmetric and can be aligned along the three coordinate axes in the cubic cuprite crystal. Thus, we consider the six linearly independent basis functions  $e^{+il\phi_x}$ ,  $e^{-il\phi_x}$ ,  $e^{+il\phi_y}$ ,  $e^{-il\phi_y}$ ,  $e^{+il\phi_z}$ ,  $e^{-il\phi_z}$ , into which  $e^{il\phi}$  can be transformed under the symmetry operations of point group  $O_h$ . For an orientation along different axes, the

number of linearly independent basis functions would differ, thus the following analysis only holds strictly for the case in which the beam axis aligns with a coordinate axis. In order to determine the symmetry of function  $e^{il\varphi}$ , we analyze how the basis functions change when undergoing  $O_h$  symmetry operations, and calculate the trace of the transformation matrix (characters). For the complete set of characters, the corresponding symmetry can be assigned according to the character tables of group  $O_h$ . The case  $l = 0$  needs to be considered separately. As  $e^{i(l=0)\varphi} = 1$ , we cannot find six linear independent basis functions, contrary to the case  $l > 0$ . The symmetry for the dipolar light field ( $l = 0$ ) is  $\Gamma_1^+$ .

A coordinate transformation of order  $n$  leads to the original coordinate after performing the transformation  $n$ -times, i.e., three times for the eight three-fold symmetry axes  $8C_3$  of group  $O_h$ :  $x \rightarrow y \rightarrow z \rightarrow x$ . It suffices to select one element per class, i.e., axis (111) in class  $8C_3$ , as all elements of the same class transform the same way. In contrast, it is important to perform the symmetry considerations for a complete basis, i.e.,  $x$ ,  $y$ , and  $z$ , in order to extract the character of a transformation (trace of transformation matrix). The complete transformations of the coordinates  $x$ ,  $y$ ,  $z$  under symmetry operations of group  $O_h$  are listed in Table S1 in the Supplementary Information. Knowing how the coordinates behave under the different symmetry operations, one can write down the transformations of the basis functions of  $e^{il\varphi}$  (see Table I).

TABLE I. Transformations of functions  $e^{\pm il\varphi_x}$ ,  $e^{\pm il\varphi_y}$ , and  $e^{\pm il\varphi_z}$  under  $O_h$  symmetry operations.

Operator $\hat{O}$	$\hat{O} e^{\pm il\varphi_x}\rangle$	$\hat{O} e^{\pm il\varphi_y}\rangle$	$\hat{O} e^{\pm il\varphi_z}\rangle$
E	$e^{\pm il\varphi_x}$	$e^{\pm il\varphi_y}$	$e^{\pm il\varphi_z}$
$8C_3$	$e^{\pm il\varphi_z}$	$e^{\pm il\varphi_x}$	$e^{\pm il\varphi_y}$
$3C_2$	$e^{\pm il(\varphi_x+\pi)}$	$e^{\mp il(\varphi_y+\pi)}$	$e^{\mp il\varphi_z}$
$6C_4$	$e^{\pm il(\varphi_x+\pi/2)}$	$e^{\mp il(\varphi_z\pm\pi/2)}$	$e^{\pm il(\varphi_y\mp\pi/2)}$
$6C_2^1$	$e^{\pm il(\varphi_y-\pi/2)}$	$e^{\pm il(\varphi_x+\pi/2)}$	$e^{\mp il(\varphi_z-\pi/2)}$

In order to calculate the transformation matrix diagonal elements, the transformed functions are decomposed into basis vectors according to  $\hat{O}|f_i\rangle = \sum_k N_{i,k}|f_k\rangle$ . The characters of the OAM light for each symmetry class are then given by the sum of the results of all six basis vectors, i.e., the trace  $\chi(\hat{O}) = Tr(N_{i,k}) = \sum_k N_{k,k}$ . The single transformation matrix diagonal elements for one representative class element of all symmetry classes of group  $O_h$  as well as the resulting character set for OAM light ( $e^{il\varphi}$ ) are listed in Table S2 in the Supplementary Information. Multiplication of the characters of  $e^{il\varphi}$  with the ones of  $A_0$  yield the character set of the complete OAM light field operator  $A = A_0 \cdot e^{il\varphi}$ . The amplitude  $A_0$  is described by symmetry  $\Gamma_1^+$ , which acts like a 1 in multiplication (identity). Further multiplication with the characters of the momentum operator  $\mathbf{p}$ , which is described by symmetry  $\Gamma_4^-$ , yields the characters of the optical transition driving operator  $A \cdot \mathbf{p}$ . The resulting character sets are listed in Table II. The assignment of symmetries is done with the help of the character and multiplication tables for symmetry group  $O_h$ . Both tables as well as additional character sets for OAM light with different amount of orbital angular momentum  $l$  as well as their symmetries are listed in the Supplementary Information in Table S2-S4.

TABLE II. Character set for OAM light field operator ( $A = A_0 \cdot e^{il\varphi}$ ) and dipole ( $A \cdot \mathbf{p} = A_0 \cdot e^{il\varphi} \cdot \mathbf{p}$ ) and quadrupole ( $A \cdot \mathbf{p} = A_0 \cdot ikz \cdot e^{il\varphi} \cdot \mathbf{p}$ ) transition driving operator for OAM light with arbitrary amount of angular momentum  $l$ .

$O_h$	E	$8C_3$	$3C_2$	$6C_4$	$6C_2'$
$A = A_0 \cdot e^{il\varphi}$	6	0	$2(-1)^l$	$2\cos(l\pi/2)$	0
$A \cdot \mathbf{p}$ (dipole)	18	0	$-2(-1)^l$	$2\cos(l\pi/2)$	0
$A \cdot \mathbf{p}$ (quadrupole)	54	0	$2(-1)^l$	$2\cos(l\pi/2)$	0

Electric quadrupole transitions require a change of two units of angular momentum ( $\Delta j = 2$ ) in matter and are sensitive to the light field gradient  $\nabla E$ . Usually, optical beams have a longitudinal field gradient, which allow for driving electric quadrupole transitions, however, with a strength of three orders of magnitude weaker than the electric dipole transition. A transverse gradient, due to the spatial structure of the beam front, such as in OAM light, can drive quadrupole transitions, too.<sup>17-23</sup> However, to make  $\Delta j > 1$  transitions similar in magnitude to standard electric dipole transitions ( $\Delta j = 1$ ), an atom usually has to be placed precisely in the vortex center (no further than an atomic size  $a_0$ ) and the probe beam has to be focused close to the diffraction limit. In contrast, the micrometer length scales of Rydberg excitons in cuprite and focused OAM beams match, hence allowing for the realization of enhanced quadrupole transitions triggered by the transverse field gradient in the center of the OAM beam (see FIG. 1 (b)).<sup>24</sup> In order to predict whether a quadrupole transition in excitons is allowed using OAM light, the symmetries of the optical transition driving operator are multiplied with the symmetry  $\Gamma_4^-$ , which accounts for the additional position vector in the quadrupole field. The resulting character set for an arbitrary amount of orbital angular momentum  $l$  is listed in Table II. More detailed information can be found in Table S2 in the Supplementary Information.

## B. Symmetry of excitons in cuprous oxide

The total symmetry of an exciton is determined by the product of valence band (hole), conduction band (electron) and envelope function (angular momentum  $l^{exc}$ ) symmetries:  $\Gamma_{exc} = \Gamma_h \times \Gamma_e \times \Gamma_{env}$ . In cuprous oxide, the electronic configurations of the single atoms (Cu and O) determine that conduction and valence band are formed from the Cu 4s and Cu 3d functions, respectively.<sup>13,26</sup> Due to the spin-orbit coupling between the quasispin  $I$  and the hole spin  $S_h$ , the sixfold degenerate valence band, having symmetry  $\Gamma_5^+$ , splits into a higher lying twofold-degenerate band of symmetry  $\Gamma_7^+$  and a lower lying fourfold-degenerate band of symmetry  $\Gamma_8^+$  by an amount of  $\Delta = 130 \text{ meV}$ .<sup>27</sup> Similarly, the Cu 4s conduction band, initially having symmetry  $\Gamma_1^+$ , splits into a higher lying fourfold-degenerate band of symmetry  $\Gamma_8^-$ , and a lower lying twofold-degenerate band of symmetry  $\Gamma_6^+$ . We consider here the yellow exciton series which occurs between the uppermost valence band ( $\Gamma_7^+$ ) and the lowest conduction band ( $\Gamma_6^+$ ) (see FIG. 1 (a)), thus  $\Gamma_{exc} = \Gamma_h \times \Gamma_e \times \Gamma_{env} = \Gamma_7^+ \times \Gamma_6^+ \times \Gamma_{env}^{l^{exc}}$ .

The symmetry property of the pure Coulomb field between electron and hole gives rise to the degeneracy of all levels with the same principal quantum number  $n$  irrespective of their angular momentum quantum number  $l^{exc}$ , which is described by the exciton envelope function, expressed in spherical harmonic functions  $Y_l^m$ .<sup>25</sup> These are listed in Table S5 in the Supplemental Information in Cartesian coordinates for  $l = 0 - 4$ . It suffices to use one representative function per orbital (symmetry group), i.e., choosing one magnetic quantum number value  $m$ ,  $Y_0^0$  for S or  $Y_1^1$  for P, to perform symmetry considerations. In the simplest case, the orbital functions are pure basis functions, so their symmetry can be directly assigned according to the character table of symmetry group  $O_h$ . The orbital functions are then irreducible representations, which is the case for S- and P-orbitals:  $Y_0^0 = 1/\sqrt{4\pi} \sim 1 \rightarrow$  S-orbital transforms as  $\Gamma_1^+$ ;  $Y_1^1 = -\sqrt{3/8\pi} \cdot (x - iy)/r \rightarrow$  P-orbital transforms as  $\Gamma_4^-$ . If the bases cannot be seen directly, one has to apply the different symmetry operations of group  $O_h$  to the orbital function and decompose them via  $N_{m_1, m_2} = \langle Y_l^{m_1} | \hat{O} | Y_l^{m_2} \rangle$ , yielding the complete character sets (shown in Table S6 in Supplementary Information). The resulting orbital symmetries, known via comparison of the character sets with the  $O_h$  character table, are shown in Table III together with the complete exciton symmetries for different envelope function. In addition, the crystal ground state has symmetry  $\Gamma_1^+$ . Therefore the transition may be allowed if the symmetry of the excitonic state appears in the decomposition of the optical transition driving operator.

TABLE III. Exciton envelope ( $\Gamma_{env}^l$ ) and total exciton transition ( $\Gamma_{exc}$ ) symmetries.<sup>16,28,29</sup>

Envelope $l^{exc}$	Exciton envelope symmetry $\Gamma_{env}^{l^{exc}}$	Exciton total symmetry $\Gamma_{exc}$
S ( $l^{exc} = 0$ )	$\Gamma_1^+$	$\Gamma_2^+ + \Gamma_5^+$
P ( $l^{exc} = 1$ )	$\Gamma_4^-$	$\Gamma_2^- + \Gamma_3^- + \Gamma_4^- + 2\Gamma_5^-$
D ( $l^{exc} = 2$ )	$\Gamma_3^+ + \Gamma_5^+$	$\Gamma_1^+ + 2\Gamma_3^+ + 3\Gamma_4^+ + \Gamma_5^+$
F ( $l^{exc} = 3$ )	$\Gamma_2^- + \Gamma_4^- + \Gamma_5^-$	$2\Gamma_1^- + \Gamma_2^- + 2\Gamma_3^- + 4\Gamma_4^- + 3\Gamma_5^-$
G ( $l^{exc} = 4$ )	$\Gamma_1^+ + \Gamma_3^+ + \Gamma_4^+ + \Gamma_5^+$	$\Gamma_1^+ + 2\Gamma_2^+ + 3\Gamma_3^+ + 4\Gamma_4^+ + 5\Gamma_5^+$

### C. Interaction of OAM light with Rydberg excitons: Modifying dipole selection rules

In Table IV the different light field operators for dipole and quadrupole OAM light are summarized. “ $l = 1$ ”- and “ $l = 3$ ”-OAM light exhibit the same symmetry. If the dipolar light field operator is of positive parity, the corresponding quadrupole light field operator is of negative parity and vice versa. For successive increase of OAM  $l$ , the parity changes alternatively. When illuminating cuprous oxide with dipolar light ( $l = 0$ ), P-excitons are visible in the absorption spectrum. According to our calculations P-excitons can also become allowed transitions in quadrupole excitation using  $l = 1$  or  $l = 3$  OAM light. In contrast, the usually dipole-forbidden S-exciton states cannot only be driven by the quadrupole field of even OAM light ( $l = 0, 2, 4$ ), but also by dipole transitions with odd OAM light ( $l = 1, 3$ ). The same holds for D- and G-excitons, while F- and H-excitons follow the excitation rules of P-excitons. These results are summarized in Table V.

TABLE IV. Symmetries of dipole ( $A_0 \cdot e^{il\varphi} \cdot \mathbf{p}$ ) and quadrupole ( $A_0 \cdot ikz \cdot e^{il\varphi} \cdot \mathbf{p}$ ) transition driving operator of OAM light with different amount of orbital angular momentum  $l$ .

Orbital angular momentum $l$	Dipole	Quadrupole
0 (even)	$\Gamma_4^-$	$\Gamma_1^+ + \Gamma_3^+ + \Gamma_4^+ + \Gamma_5^+$
1 (odd)	$\Gamma_1^+ + \Gamma_2^+ + 2\Gamma_3^+ + 2\Gamma_4^+ + 2\Gamma_5^+$	$2\Gamma_1^- + 2\Gamma_2^- + 4\Gamma_3^- + 7\Gamma_4^- + 7\Gamma_5^-$
2 (even)	$\Gamma_2^- + \Gamma_3^- + 2\Gamma_4^- + 3\Gamma_5^-$	$2\Gamma_1^+ + 3\Gamma_2^+ + 5\Gamma_3^+ + 6\Gamma_4^+ + 7\Gamma_5^+$
3 (odd)	$\Gamma_1^+ + \Gamma_2^+ + 2\Gamma_3^+ + 2\Gamma_4^+ + 2\Gamma_5^+$	$2\Gamma_1^- + 2\Gamma_2^- + 4\Gamma_3^- + 7\Gamma_4^- + 7\Gamma_5^-$
4 (even)	$\Gamma_1^- + \Gamma_3^- + 3\Gamma_4^- + 2\Gamma_5^-$	$3\Gamma_1^+ + 2\Gamma_2^+ + 5\Gamma_3^+ + 7\Gamma_4^+ + 6\Gamma_5^+$

TABLE V. Exciton transition symmetries and OAM light they can be excited with.

Envelope $l^{exc}$	Exciton total symmetry $\Gamma_{exc}$	Parity	$l^{dipole}$	$l^{quadrupole}$
S	$\Gamma_2^+ + \Gamma_5^+$	+	odd	even
P	$\Gamma_2^- + \Gamma_3^- + \Gamma_4^- + 2\Gamma_5^-$	-	even	odd
D	$\Gamma_1^+ + 2\Gamma_3^+ + 3\Gamma_4^+ + \Gamma_5^+$	+	odd	even
F	$2\Gamma_1^- + \Gamma_2^- + 2\Gamma_3^- + 4\Gamma_4^- + 3\Gamma_5^-$	-	even	odd
G	$\Gamma_1^+ + 2\Gamma_2^+ + 3\Gamma_3^+ + 4\Gamma_4^+ + 5\Gamma_5^+$	+	odd	even
H	$\Gamma_1^- + 2\Gamma_2^- + 4\Gamma_3^- + 5\Gamma_4^- + 6\Gamma_5^-$	-	even	odd

#### D. Exciton and Light Mode Spatial Extensions

We would like to predict for which principal quantum number  $n$  a Rydberg exciton in cuprous oxide would most likely interact with focused OAM light, due to their largest spatial overlap. Therefore, the S-exciton envelope wavefunctions are visualized as a function of  $n$  and their spatial overlap with a light mode of  $l = 1$  orbital angular momentum is discussed. The excitonic radial wave function  $r^2 R_{Cu_2O}^2(r)$  is calculated in analogy to the hydrogen radial wave function  $R_{nl}$  and the light mode spatial extension is calculated based on the formula for Laguerre-Gauss modes for  $l = 1$  at the focal point  $z = 0$ :  $|u_{l=1}^{p=0}(r, \varphi = 0, z = 0)|^2$ . The results are shown in FIG. 2 for S-exciton states with principal quantum number  $n = 9 - 14$ . From here we see that S-exciton states with principal quantum number  $n = 12$  show the largest overlap with the spatial mode of  $l = 1$  OAM light when focused down to a spot of  $w_0 = 250 \text{ nm}$  beam waist, which corresponds to a radius  $r = 497 \text{ nm}$ . See Supplementary Information for more details.

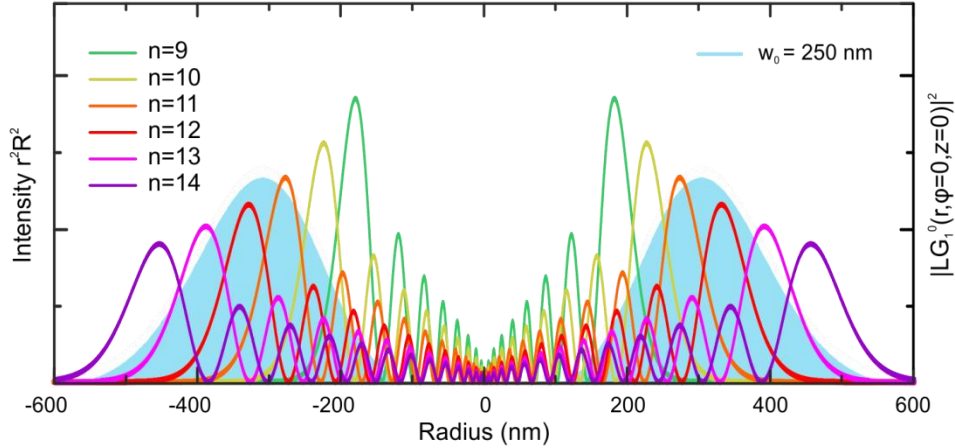


FIG. 2. Visualization of the spatial overlap between exciton states and a Laguerre-Gauss mode. The S-exciton ( $l^{exc} = 0$ ) radial wave function  $r^2 R_{Cu_2O}^2$  is plotted for different quantum states  $n = 9 - 14$ . The intensity distribution of the Laguerre-Gauss mode ( $l = 1$ ) is shown for a beam waist  $w_0 = 250 \text{ nm}$ .

#### IV. CONCLUSION AND OUTLOOK

In the present paper we have given a detailed analysis of orbital angular momentum (OAM) light and exciton symmetries in cuprite. The symmetries of OAM light with different amount of OAM  $l$  as well as the symmetries of excitons with different envelope functions (angular momentum quantum number  $l^{exc}$ ) have been calculated. Comparing their overlap with the dipole selection rules allows us to predict that the alteration of the OAM of light may enable one to modify the optical transition selection rules and, hence, to excite usually dipole-forbidden Rydberg excitons in  $\text{Cu}_2\text{O}$ . We find that S- and D-envelope wavefunction excitons should be excitable with  $l = 1$  and  $l = 3$  OAM light. The precise oscillator strength of the transitions, however, requires further detailed theoretical investigation.

Using group-theoretical methods, we propose a new method for the observation of dipole-forbidden excitons in cuprite. In order to test the predictions we would like to implement the corresponding experiment as follows: Orbital angular momentum light can be created by imprinting a phaseplate (pp) on a fiber facet.<sup>30</sup> Upon transmission through the phaseplate, a beam of wavelength  $\lambda$  is subjected to a phase delay  $\psi$  which depends on the azimuthal angle  $\varphi$ , where  $\psi = (n_{pp} - n_0) \cdot s \cdot \varphi / \lambda$  ( $s$ : step height,  $n_0$ : refractive index of the surrounding material). A screw phase-dislocation produced on-axis causes destructive interference leading to the characteristic ring intensity pattern in the far field. For a pure Laguerre-Gauss mode the total phase delay around the phaseplate must be an integer multiple of  $2\pi$ , thus the physical step height in the spiral phaseplate is given by  $s = l \cdot \lambda / (n_{pp} - n_0)$ . The purity of Laguerre-Gaussian modes is limited by the co-production of higher order

modes. This OAM light is then focused for example by a Fresnel lens carved into the Cu<sub>2</sub>O crystal, and transmission measurements are performed. We are going to analyze the different transition probabilities as set of quantum number  $n$ , exciton envelope wavefunction (angular momentum quantum number  $l^{exc}$ ), as well as orbital angular momentum quantum number  $l$ . In addition, we want to calculate the transition matrix elements and oscillator strength using DFT. Then we would also be able to predict how probable an allowed transition will be.

## ACKNOWLEDGEMENTS

We gratefully acknowledge funding by the Deutsche Forschungsgemeinschaft (DFG) (SPP 1929 GiRyd) and the European Research Council (ERC) (Complexplas). Discussions with T. Pfau, M. M. Glazov, and J. Heckötter are acknowledged.

## REFERENCES

1. G. M. Kavoulakis, Y.-Ch. Chung, and G. Baym, "Fine structure of excitons in Cu<sub>2</sub>O," *Phys. Rev. B* **55**, 7593 (1997).
2. J. L. Deiss and A. Daunois, "Modulated exciton spectroscopy," *Surface science* **37**, 804-827 (1973).
3. F. Schöne, S.-O. Krüger, P. Grünwald, M. Aßmann, J. Heckötter, J. Thewes, H. Stolz, D. Fröhlich, M. Bayer, and S. Scheel, "Coupled valence band dispersions and the quantum defect of excitons in Cu<sub>2</sub>O," *J. Phys. B* **49**, 134003 (2016).
4. T. Kazimierczuk, D. Fröhlich, S. Scheel, H. Stolz, and M. Bayer, "Giant Rydberg excitons in the copper oxide Cu<sub>2</sub>O," *Nature* **514**, 343-347 (2014).
5. S. O. Krüger and S. Scheel, "Waveguides for Rydberg excitons in Cu<sub>2</sub>O from strain traps," *Phys Rev B* **97**, 205208 (2018).
6. T. Inui, Y. Tanabe, and Y. Onodera, *Group theory and its applications in physics* (Springer, 1996).
7. N. B. Simpson, K. Dholakia, L. Allen, and M. J. Padgett, "Mechanical equivalence of spin and orbital angular momentum of light: an optical spanner," *Opt. Lett.* **22**, 52-54 (1997).
8. M. Padgett, J. Courtial, and L. Allen, "Light's Orbital Angular Momentum," *Physics today* **57**, 35-40 (2004)
9. Y. Yan and A. E. Willner, "Efficient generation and multiplexing of optical orbital angular momentum modes in a ring fiber by using multiple coherent inputs," *Opt. Lett.* **37**, 3645-3647 (2012).
10. G. A. Turnbull, D. A. Robertson, G. M. Smith, L. Allen, and M. J. Padgett, "The generation of free-space Laguerre-Gaussian modes at millimetre-wave frequencies by use of a spiral phaseplate," *Opt. Commun.* **127**, 183-188 (1996).
11. N. R. Heckenberg, R. McDuff, C. P. Smith, H. Rubinsztein-Dunlop, and M. J. Wegener, "Laser beams with phase singularities," *Optical and Quantum Electronics* **24**, S951-S962 (1992).
12. G. F. Koster, J. O. Dimmock, R. G. Wheeler, and H. Statz, *Properties of the thirty-two point groups* (M.I.T. Press Research Monographs, 1963).
13. R. J. Elliott, "Symmetry of excitons in Cu<sub>2</sub>O," *Phys. Rev.* **124**, 340 (1961).
14. R. S. Knox and A. Gold, *Symmetry in the solid state* (W. A. Benjamin Inc., 1964).
15. A. Werner and H. D. Hochheimer, "High-pressure x-ray study of Cu<sub>2</sub>O and Ag<sub>2</sub>O," *Phys. Rev. B* **25**, 5929 (1982).
16. J. Thewes, J. Heckötter, T. Kazimierczuk, M. Aßmann, D. Fröhlich, M. Bayer, M. A. Semina, and M. M. Glazov, "Observation of high angular momentum excitons in cuprous oxide," *PRL* **115**, 027402 (2015).
17. Ch. T. Schmiegelow, J. Schulz, H. Kaufmann, T. Ruster, U. G. Poschinger, and F. Schmidt-Kaler, "Transfer of optical orbital angular momentum to a bound electron," *Nature Commun.* **7**, 12998 (2016).
18. S. Franke-Arnold, "Optical angular momentum and atoms," *Phil. Trans. R. Soc. A* **375**, 20150435 (2017).
19. A. Afanasev, "High-multipole excitations of hydrogen-like atoms by twisted photons near a phase singularity," *J. Opt.* **18**, 074013 (2016).
20. V. E. Lembessis and M. Babiker, "Enhanced quadrupole effects for atoms in optical vortices," *PRL* **110**, 083002 (2013).
21. S. Lloyd, M. Babiker, and J. Yuan, "Interaction of electron vortices and optical vortices with matter and processes of orbital angular momentum exchange," *Phys. Rev. A* **86**, 023816 (2012).
22. F. Machado, N. Rivera, H. Buljan, M. Soljačić, and I. Kaminer, "Shaping polaritons to reshape selection rules," *ACS Photonics* **5**, 3064-3072 (2017).
23. G. F. Quinteiro, F. Schmidt-Kaler, C.T. Schmiegelow, "Twisted-light-ion interaction: The role of longitudinal fields," *Phys. Rev. Lett* **119**, 253203 (2017).
24. A. Youjji, S. Saito, and A. Otomo, "Creation of Excitons Excited by Light with a Spatial Mode," *J. Phys. Soc. Jpn.* **86**, 124720 (2017).
25. V. Heine, *Group theory in quantum mechanics* (Pergamon, 1960).
26. J. W. Hodby, T. E. Jenkins, C. Schwab, H. Tamura, and D. Trivich, "Cyclotron resonance of electrons and of holes in cuprous oxide," *Cu<sub>2</sub>O, J. Phys. C* **9**, 1429 (1976).
27. F. Schweiner, J. Main, and G. Wunner G, "Magnetoexcitons in cuprous oxide," *Phys Rev B* **95**, 035202 (2017).
28. J. C. Merle, C. Wecker, A. Daunois, J. L. Deiss, and S. Nikitine, "Modulated excitonic absorption on Cu<sub>2</sub>O in magnetic or parallel electric and magnetic fields," *Surface Science* **37**, 347-354 (1973).
29. J. Heckötter, M. Freitag, M. Aßmann, M. Bayer, M. A. Semina, and M. M. Glazov, "High resolution study of the yellow excitons in Cu<sub>2</sub>O subject to an electric field," *Phys. Rev. B* **95**, 035210 (2017).
30. K. Weber, F. Hütt, S. Thiele, T. Gissibl, A. Herkommer, and H. Giessen, "Single mode fiber based delivery of OAM light by 3D direct laser writing," *Opt. Express* **25**, 19672-19679 (2017).

## Supplementary Information

### I. $O_h$ SYMMETRY GROUP

Cuprous oxide belongs to symmetry group  $O_h$ , which is of order 48 and contains all operations which transform a cube into itself. The 24 proper rotations are in the classes E: identity;  $8C_3$ : rotations of  $2\pi/3$  about the eight threefold space diagonal axes  $\langle 111 \rangle$ ,  $\langle -1-1-1 \rangle$ ,  $\langle 11-1 \rangle$ ,  $\langle -1-11 \rangle$ ,  $\langle 1-11 \rangle$ ,  $\langle -11-1 \rangle$ ,  $\langle -111 \rangle$ ,  $\langle 1-1-1 \rangle$ ;  $3C_2$ : rotations of  $\pi$  about the three cubic coordinate axes  $\langle 100 \rangle$ ,  $\langle 010 \rangle$ ,  $\langle 001 \rangle$ ;  $6C_4$ : rotations of  $\pi/2$  about the cubic coordinate axes  $\langle 100 \rangle$ ,  $\langle -100 \rangle$ ,  $\langle 010 \rangle$ ,  $\langle 0-10 \rangle$ ,  $\langle 001 \rangle$ ,  $\langle 00-1 \rangle$ ;  $6C_2'$ : rotations of  $\pi$  about the six twofold face diagonal axes  $\langle 110 \rangle$ ,  $\langle 1-10 \rangle$ ,  $\langle 101 \rangle$ ,  $\langle 10-1 \rangle$ ,  $\langle 011 \rangle$ ,  $\langle 01-1 \rangle$  (see FIG. S1). The 24 improper rotations are I: inversion;  $8S_6$ : rotations through  $\pi/3$  about the eight space diagonal axes followed by a reflection in the plane perpendicular to the axis of rotation;  $3\sigma_h$ : reflection in a plane perpendicular to the principal axis of symmetry, i.e. xy-plane (ts0), xz-plane (t0r), yz-plane (0sr);  $6S_4$ : rotations through  $\pi/2$  about the six coordinate axes followed by a reflection in the plane perpendicular to the axis of rotation;  $6\sigma_d$ : reflection containing a principal axis of symmetry that bisects the angle between two two-fold rotation axes perpendicular to the principal axis, i.e.,  $\pm 45^\circ$  to xy-, xz-, and yz-plane (tvv), (tv-v), (usu), (us-u), (wwr), (w-wr).<sup>14</sup>

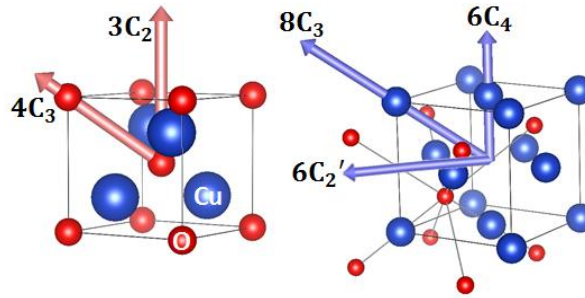


FIG. S1.  $Cu_2O$  crystal lattice. O atoms (red) form a bcc lattice, Cu atoms (blue) form a fcc lattice. The rotational operations of the crystallographic groups T and  $O$  fit to the positions of the O- and Cu-atoms respectively. The number of similar operations are written in front of the rotation symbol.

### II. COORDINATE TRANSFORMATIONS UNDER $O_h$ SYMMETRY OPERATIONS

TABLE S1. Coordinate transformations under  $O_h$  symmetry operations.

Operator $\hat{O}$	Vector	$x$	$y$	$z$
E		$x \rightarrow x$	$y \rightarrow y$	$z \rightarrow z$
$8C_3$	(111)	$x \rightarrow y \rightarrow z \rightarrow x$	$y \rightarrow z \rightarrow x \rightarrow y$	$z \rightarrow x \rightarrow y \rightarrow z$
	(-1-1-1)	$x \rightarrow z \rightarrow y \rightarrow x$	$y \rightarrow x \rightarrow z \rightarrow y$	$z \rightarrow y \rightarrow x \rightarrow z$
	(-111)	$x \rightarrow -z \rightarrow -y \rightarrow x$	$y \rightarrow -x \rightarrow z \rightarrow y$	$z \rightarrow y \rightarrow -x \rightarrow z$
	(1-1-1)	$x \rightarrow -y \rightarrow -z \rightarrow x$	$y \rightarrow z \rightarrow -x \rightarrow y$	$z \rightarrow -x \rightarrow y \rightarrow z$
	(1-11)	$x \rightarrow -y \rightarrow z \rightarrow x$	$y \rightarrow -z \rightarrow -x \rightarrow y$	$z \rightarrow x \rightarrow -y \rightarrow z$
	(-11-1)	$x \rightarrow z \rightarrow -y \rightarrow x$	$y \rightarrow -x \rightarrow -z \rightarrow y$	$z \rightarrow -y \rightarrow x \rightarrow z$
	(11-1)	$x \rightarrow -z \rightarrow -y \rightarrow x$	$y \rightarrow x \rightarrow -z \rightarrow y$	$z \rightarrow -y \rightarrow -x \rightarrow z$
	(-1-11)	$x \rightarrow -y \rightarrow -z \rightarrow x$	$y \rightarrow -z \rightarrow x \rightarrow y$	$z \rightarrow -x \rightarrow -y \rightarrow z$
$3C_2$	(100)	$x \rightarrow x \rightarrow x$	$y \rightarrow -y \rightarrow y$	$z \rightarrow -z \rightarrow z$
	(010)	$x \rightarrow -x \rightarrow x$	$y \rightarrow y \rightarrow y$	$z \rightarrow -z \rightarrow z$
	(001)	$x \rightarrow -x \rightarrow x$	$y \rightarrow -y \rightarrow y$	$z \rightarrow z \rightarrow z$
$6C_4$	X	$x \rightarrow x \rightarrow x \rightarrow x \rightarrow x$	$y \rightarrow -z \rightarrow -y \rightarrow z \rightarrow y$	$z \rightarrow y \rightarrow -z \rightarrow -y \rightarrow z$
	-X	$x \rightarrow x \rightarrow x \rightarrow x \rightarrow x$	$y \rightarrow z \rightarrow -y \rightarrow -z \rightarrow y$	$z \rightarrow -y \rightarrow -z \rightarrow y \rightarrow z$
	Y	$x \rightarrow z \rightarrow -x \rightarrow -z \rightarrow x$	$y \rightarrow y \rightarrow y \rightarrow y \rightarrow y$	$z \rightarrow -x \rightarrow -z \rightarrow x \rightarrow z$
	-Y	$x \rightarrow -z \rightarrow -x \rightarrow z \rightarrow x$	$y \rightarrow y \rightarrow y \rightarrow y \rightarrow y$	$z \rightarrow x \rightarrow -z \rightarrow -x \rightarrow z$
	Z	$x \rightarrow -y \rightarrow -x \rightarrow y \rightarrow x$	$y \rightarrow x \rightarrow -y \rightarrow -x \rightarrow y$	$z \rightarrow z \rightarrow z \rightarrow z \rightarrow z$
	-Z	$x \rightarrow y \rightarrow -x \rightarrow -y \rightarrow x$	$y \rightarrow -x \rightarrow -y \rightarrow x \rightarrow y$	$z \rightarrow z \rightarrow z \rightarrow z \rightarrow z$
$6C_2'$	(110)	$x \rightarrow y \rightarrow x$	$y \rightarrow x \rightarrow y$	$z \rightarrow -z \rightarrow z$
	(1-10)	$x \rightarrow -y \rightarrow x$	$y \rightarrow -x \rightarrow y$	$z \rightarrow -z \rightarrow z$
	(101)	$x \rightarrow z \rightarrow x$	$y \rightarrow -y \rightarrow y$	$z \rightarrow x \rightarrow z$
	(10-1)	$x \rightarrow -z \rightarrow x$	$y \rightarrow -y \rightarrow y$	$z \rightarrow -x \rightarrow z$
	(011)	$x \rightarrow -x \rightarrow x$	$y \rightarrow z \rightarrow y$	$z \rightarrow y \rightarrow z$
	(01-1)	$x \rightarrow -x \rightarrow x$	$y \rightarrow -z \rightarrow y$	$z \rightarrow -y \rightarrow z$

### III. TRANSFORMATION MATRIX DIAGONAL ELEMENTS AND RESULTING CHARACTERS

TABLE S2. Matrix elements of the transformation matrices  $Op. |f_i\rangle = \sum_k N_{i,k} |f_k\rangle$  and their common characters for OAM light  $e^{il\varphi}$  with arbitrary amount of angular momentum  $l$ , as well as character sets for OAM light field operator  $A = A_0 \cdot e^{il\varphi}$  and OAM dipole ( $A \cdot p = A_0 \cdot e^{il\varphi} \cdot p$ ) and quadrupole ( $A \cdot p = A_0 \cdot ikz \cdot e^{il\varphi} \cdot p$ ) transition driving operator.

$O_h$	E	$8C_3$	$3C_2$	$6C_4$	$6C_2'$	I	$8S_6$	$3\sigma_h$	$6S_4$	$6\sigma_d$
$e^{+il\varphi_x}$	1	0	$e^{+il\pi}$	$e^{+il\pi/2}$	0	$e^{+il\pi}$	0	1	$e^{+il\pi/2}$	0
$e^{-il\varphi_x}$	1	0	$e^{+il\pi}$	$e^{+il\pi/2}$	0	$e^{+il\pi}$	0	1	$e^{+il\pi/2}$	0
$e^{+il\varphi_y}$	1	0	0	0	0	$e^{+il\pi}$	0	0	0	0
$e^{-il\varphi_y}$	1	0	0	0	0	$e^{+il\pi}$	0	0	0	0
$e^{+il\varphi_z}$	1	0	0	0	0	$e^{+il\pi}$	0	0	0	0
$e^{-il\varphi_z}$	1	0	0	0	0	$e^{+il\pi}$	0	0	0	0
$e^{il\varphi}$ (Sum)	6	0	$2(-1)^l$	$2\cos(l\pi/2)$	0	$6(-1)^l$	0	2	$2\cos(l\pi/2)$	0
$A_0$	1	1	1	1	1	1	1	1	1	1
$A = A_0 \cdot e^{il\varphi}$	6	0	$2(-1)^l$	$2\cos(l\pi/2)$	0	$6(-1)^l$	0	2	$2\cos(l\pi/2)$	0
$l = 1$	6	0	-2	0	0	-6	0	2	0	0
$l = 2$	6	0	2	-2	0	6	0	2	-2	0
$l = 3$	6	0	-2	0	0	-6	0	2	0	0
$l = 4$	6	0	2	2	0	6	0	2	2	0
$p$	3	0	-1	1	-1	-3	0	1	-1	1
$A \cdot p$ (dipole)	18	0	$-2(-1)^l$	$2\cos(l\pi/2)$	0	$-18(-1)^l$	0	2	$-2\cos(l\pi/2)$	0
$l = 1$	18	0	2	0	0	18	0	2	0	0
$l = 2$	18	0	-2	-2	0	-18	0	2	2	0
$l = 3$	18	0	2	0	0	18	0	2	0	0
$l = 4$	18	0	-2	2	0	-18	0	2	-2	0
$z$	3	0	-1	1	-1	-3	0	1	-1	1
$A \cdot p$ (quadrupole)	54	0	$2(-1)^l$	$2\cos(l\pi/2)$	0	$54(-1)^l$	0	2	$2\cos(l\pi/2)$	0
$l = 1$	54	0	-2	0	0	-54	0	2	0	0
$l = 2$	54	0	2	-2	0	54	0	2	-2	0
$l = 3$	54	0	-2	0	0	-54	0	2	0	0
$l = 4$	54	0	2	2	0	54	0	2	2	0

### IV. CHARACTER TABLE AND BASIS FUNCTIONS FOR THE GROUP $O_H$

TABLE S3. Character table and basis functions for the group  $O_h$ .<sup>12</sup>

$O_h$	E	$8C_3$	$3C_2$	$6C_4$	$6C_2'$	I	$8S_6$	$3\sigma_h$	$6S_4$	$6\sigma_d$	Bases
$\Gamma_1^+$	1	1	1	1	1	1	1	1	1	1	R
$\Gamma_2^+$	1	1	1	-1	-1	1	1	1	-1	-1	$(x^2 - y^2)(y^2 - z^2)(z^2 - x^2)$
$\Gamma_3^+$	2	-1	2	0	0	2	-1	2	0	0	$(2z^2 - x^2 - y^2), \sqrt{3}(x^2 - y^2)$
$\Gamma_4^+$	3	0	-1	1	-1	3	0	-1	1	-1	$S_x, S_y, S_z$
$\Gamma_5^+$	3	0	-1	-1	1	3	0	-1	-1	1	$yz, xz, xy$
$\Gamma_1^-$	1	1	1	1	1	-1	-1	-1	-1	-1	$\Gamma_2^- \times \Gamma_2^+$
$\Gamma_2^-$	1	1	1	-1	-1	-1	-1	-1	1	1	$xyz$
$\Gamma_3^-$	2	-1	2	0	0	-2	1	-2	0	0	$\Gamma_3^+ \times \Gamma_2^-$
$\Gamma_4^-$	3	0	-1	1	-1	-3	0	1	-1	1	$x, y, z$
$\Gamma_5^-$	3	0	-1	-1	1	-3	0	1	1	-1	$\Gamma_5^+ \times \Gamma_1^-$
$\Gamma_6^+$	2	1	0	$\sqrt{2}$	0	2	1	0	$\sqrt{2}$	0	$\phi(1/2, -1/2), \phi(1/2, 1/2)$
$\Gamma_7^+$	2	1	0	$-\sqrt{2}$	0	2	1	0	$-\sqrt{2}$	0	$\Gamma_6^+ \times \Gamma_2^+$
$\Gamma_8^+$	4	-1	0	0	0	-4	-1	0	0	0	$\phi(3/2, -3/2), \phi(3/2, -1/2), \phi(3/2, 1/2), \phi(3/2, 3/2)$
$\Gamma_6^-$	2	1	0	$\sqrt{2}$	0	-2	-1	0	$-\sqrt{2}$	0	$\Gamma_6^+ \times \Gamma_1^-$
$\Gamma_7^-$	2	1	0	$-\sqrt{2}$	0	-2	-1	0	$\sqrt{2}$	0	$\Gamma_6^+ \times \Gamma_2^-$
$\Gamma_8^-$	4	-1	0	0	0	-4	1	0	0	0	$\Gamma_8^+ \times \Gamma_1^-$



## V. MULTIPLICATION TABLE FOR THE GROUPS O AND T<sub>D</sub>.

TABLE S4. Multiplication table for the groups O and T<sub>d</sub>. Group O<sub>h</sub> is augmented by taking into account parity.<sup>12</sup>

$\Gamma_1$	$\Gamma_2$	$\Gamma_3$	$\Gamma_4$	$\Gamma_5$	$\Gamma_6$	$\Gamma_7$	$\Gamma_8$	$\times$
$\Gamma_1$	$\Gamma_2$	$\Gamma_3$	$\Gamma_4$	$\Gamma_5$	$\Gamma_6$	$\Gamma_7$	$\Gamma_8$	$\Gamma_1$
	$\Gamma_1$	$\Gamma_3$	$\Gamma_5$	$\Gamma_4$	$\Gamma_7$	$\Gamma_6$	$\Gamma_8$	$\Gamma_2$
		$\Gamma_1 + \Gamma_2 + \Gamma_3$	$\Gamma_4 + \Gamma_5$	$\Gamma_4 + \Gamma_5$	$\Gamma_8$	$\Gamma_8$	$\Gamma_6 + \Gamma_7 + \Gamma_8$	$\Gamma_3$
			$\Gamma_1 + \Gamma_3 + \Gamma_4 + \Gamma_5$	$\Gamma_2 + \Gamma_3 + \Gamma_4 + \Gamma_5$	$\Gamma_6 + \Gamma_8$	$\Gamma_7 + \Gamma_8$	$\Gamma_6 + \Gamma_7 + 2\Gamma_8$	$\Gamma_4$
				$\Gamma_1 + \Gamma_3 + \Gamma_4 + \Gamma_5$	$\Gamma_7 + \Gamma_8$	$\Gamma_6 + \Gamma_8$	$\Gamma_6 + \Gamma_7 + 2\Gamma_8$	$\Gamma_5$
					$\Gamma_1 + \Gamma_4$	$\Gamma_2 + \Gamma_5$	$\Gamma_3 + \Gamma_4 + \Gamma_5$	$\Gamma_6$
						$\Gamma_1 + \Gamma_4$	$\Gamma_3 + \Gamma_4 + \Gamma_5$	$\Gamma_7$
							$\Gamma_1 + \Gamma_2 + \Gamma_3 + 2\Gamma_4 + 2\Gamma_5$	$\Gamma_8$

## VI. SPHERICAL HARMONICS AS EXCITON ENVELOPE FUNCTIONS

TABLE S5. Spherical harmonics functions in Cartesian coordinates.

$l$	0	1	2	3	4
$m$	S-exciton env.	P-exciton env.	D-exciton env.	F-exciton env.	G-exciton envelope
-4					$Y_4^{-4}(\theta, \varphi) = \frac{3}{16\sqrt{2\pi}} \frac{(x-iy)^4}{r^4}$
-3				$Y_3^{-3}(\theta, \varphi) = \frac{1}{8\sqrt{\pi}} \frac{35(x-iy)^3 z}{r^3}$	$Y_4^{-3}(\theta, \varphi) = \frac{3}{8\sqrt{\pi}} \frac{35(x-iy)^2 z}{r^4}$
-2			$Y_2^{-2}(\theta, \varphi) = \frac{1}{4\sqrt{2\pi}} \frac{15(x-iy)^2 z}{r^2}$	$Y_3^{-2}(\theta, \varphi) = \frac{1}{4\sqrt{2\pi}} \frac{105(x-iy)^2 z}{r^3}$	$Y_4^{-2}(\theta, \varphi) = \frac{3}{8\sqrt{2\pi}} \frac{5(x-iy)^2(7z^2-r^2)}{r^4}$
-1		$Y_1^{-1}(\theta, \varphi) = \frac{1}{2\sqrt{2\pi}} \frac{3(x-iy)}{r}$	$Y_2^{-1}(\theta, \varphi) = \frac{1}{2\sqrt{2\pi}} \frac{15(x-iy)z}{r^2}$	$Y_3^{-1}(\theta, \varphi) = \frac{1}{8\sqrt{\pi}} \frac{21(x-iy)(4z^2-x^2-y^2)}{r^3}$	$Y_4^{-1}(\theta, \varphi) = \frac{3}{8\sqrt{\pi}} \frac{5(x-iy)z(7z^2-3r^2)}{r^4}$
0	$Y_0^0(\theta, \varphi) = \frac{1}{2\sqrt{\pi}}$	$Y_1^0(\theta, \varphi) = \frac{1}{2\sqrt{\pi}} \frac{z}{r}$	$Y_2^0(\theta, \varphi) = \frac{1}{4\sqrt{2\pi}} \frac{5(2z^2-x^2-y^2)}{r^2}$	$Y_3^0(\theta, \varphi) = \frac{1}{4\sqrt{2\pi}} \frac{7z(2z^2-3x^2-3y^2)}{r^3}$	$Y_4^0(\theta, \varphi) = \frac{1}{4\sqrt{\pi}} \frac{7z(2z^2-3x^2-3y^2)}{r^4}$
1		$Y_1^1(\theta, \varphi) = \frac{1}{2\sqrt{2\pi}} \frac{3(x+iy)}{r}$	$Y_2^1(\theta, \varphi) = -\frac{1}{2\sqrt{2\pi}} \frac{15(x+iy)z}{r^2}$	$Y_3^1(\theta, \varphi) = -\frac{1}{8\sqrt{\pi}} \frac{21(x+iy)(4z^2-x^2-y^2)}{r^3}$	$Y_4^1(\theta, \varphi) = -\frac{3}{8\sqrt{\pi}} \frac{5(x+iy)z(7z^2-3r^2)}{r^4}$
2			$Y_2^2(\theta, \varphi) = \frac{1}{4\sqrt{2\pi}} \frac{15(x+iy)^2 z}{r^2}$	$Y_3^2(\theta, \varphi) = \frac{1}{4\sqrt{2\pi}} \frac{105(x+iy)^2 z}{r^3}$	$Y_4^2(\theta, \varphi) = \frac{3}{8\sqrt{2\pi}} \frac{5(x+iy)^2(7z^2-r^2)}{r^4}$
3				$Y_3^3(\theta, \varphi) = -\frac{1}{8\sqrt{\pi}} \frac{35(x+iy)^3 z}{r^3}$	$Y_4^3(\theta, \varphi) = -\frac{3}{8\sqrt{\pi}} \frac{35(x+iy)^3 z}{r^4}$
4					$Y_4^4(\theta, \varphi) = \frac{3}{16\sqrt{2\pi}} \frac{35(x+iy)^4}{r^4}$

## VII. EXCITON ENVELOPE FUNCTION CHARACTER SETS AND SYMMETRIES

TABLE S6. Character sets and symmetries of exciton envelope functions.

Envelope $l^{exc}$	E (000)	8C <sub>3</sub> (111)	3C <sub>2</sub> (100)	6C <sub>4</sub> (X)	6C <sub>2</sub> ' (110)	Exciton envelope symmetry $\Gamma_{env}^{l^{exc}}$
S ( $l^{exc} = 0$ )	1	1	1	1	1	$\Gamma_1^+$
P ( $l^{exc} = 1$ )	3	0	-1	1	-1	$\Gamma_4^-$
D ( $l^{exc} = 2$ )	5	-1	1	-1	1	$\Gamma_3^+ + \Gamma_5^+$
F ( $l^{exc} = 3$ )	7	1	-1	-1	-1	$\Gamma_2^- + \Gamma_4^- + \Gamma_5^-$
G ( $l^{exc} = 4$ )	9	0	1	1	1	$\Gamma_1^+ + \Gamma_3^+ + \Gamma_4^+ + \Gamma_5^+$

### 7. Exciton and light mode spatial extensions

Exciton radial wave function:

$$R_{Cu_2O} = \frac{2}{n^2} \sqrt{\frac{(n-l-1)!}{(n+l)!^3}} e^{-\frac{\alpha_{Cu_2O} r}{z}} (\alpha_{Cu_2O} r)^l (-1)^{2l+1} \left( \frac{1}{\alpha_{Cu_2O}} \right)^{2l-1} \frac{\partial^{2l+1}}{\partial r^{2l+1}} \left( e^{\alpha_{Cu_2O} r} \left( \frac{1}{\alpha_{Cu_2O}} \right)^{n+l} \frac{\partial^{n+l}}{\partial r^{n+l}} (e^{-\alpha_{Cu_2O} r} (\alpha_{Cu_2O} r)^{n+l}) \right) \quad (S1)$$

$n$ : principal quantum number;  $l$ : OAM quantum number;  $\alpha_{Cu_2O} = \frac{2 \cdot m^* / m_0}{\varepsilon \cdot a_0 \cdot n} = \frac{2 \cdot 0.4}{9.8 \cdot a_0 \cdot n}$ ;  $a_0 = \frac{4\pi \cdot \varepsilon_0 \cdot \hbar^2}{m_0 \cdot e^2}$ : Bohr radius.

Laguerre-Gauss mode:

$$u_l^p(r, \varphi, z) = \frac{C_{lp}^{LG}}{w(z)} \left( \frac{r\sqrt{2}}{w(z)} \right)^{|l|} e^{-\frac{r^2}{w^2(z)}} L_l^p \left( \frac{2r^2}{w^2(z)} \right) e^{-ik\frac{r^2}{2R(z)}} e^{i\varphi} e^{i\psi(z)} \quad (S2)$$

At the focus  $z = 0$ :  $R(z = 0) = \infty$  and  $e^{-ik\frac{r^2}{2R(z=0)}} = 1$ , as well as  $\psi(z = 0) = \arctan(0) = 0$  and  $e^{i\psi(z=0)} = 1$ , and  $w(z = 0) = w_0$ . Furthermore, we set  $p = 0$ :  $L_l^{p=0} = 1$  and  $C_{lp}^{LG} = \sqrt{\frac{2p!}{\pi(p+|l|)!}} \rightarrow \sqrt{\frac{2}{\pi|l|!}}$ . The Laguerre-Gauss mode for  $l = 1$  then becomes:

$$u_1^0(r, \varphi, z = 0) = \frac{4r^3}{\sqrt{\pi} w_0^4} \cdot e^{-\frac{r^2}{w_0^2}} \cdot e^{i\varphi} \quad (S3)$$

As the mode is cylindrically symmetric, we set  $\varphi = 0$  and plot the intensity distribution given by the absolute value squared as a function of  $r$ ,  $|u_{l=1}^{p=0}(r, \varphi = 0, z = 0)|^2$ , for a beam waist  $w_0 = 250 \text{ nm}$ . The beam waist here refers to the thickness of the Laguerre-Gauss ring. We evaluate the maximum of the intensity cross section curve  $\text{Max}|u_{l=1}^{p=0}(r, \varphi = 0, z = 0)|^2$  and calculate the radius at which the function is decayed to the  $1/e^2$  of its maximum value, which we then define as the radius of the Laguerre-Gauss mode. For a beam waist  $w_0 = 250 \text{ nm}$  this gives a radius  $r = 497 \text{ nm}$ .